Journal of Geophysical Research: Space Physics

RESEARCH ARTICLE
10.1002/2017JA024593

# Statistical Properties of Plasmaspheric Hiss From Van Allen Probes Observations

D. P. Hartley[1], C. A. Kletzing[1], O. Santolík[2,3], L. Chen[4], and R. B. Horne[5]

[1]Department of Physics and Astronomy, University of Iowa, Iowa City, IA, USA, [2]Department of Space Physics, Institute of Atmospheric Physics, Prague, Czech Republic, [3]Faculty of Mathematics and Physics, Charles University, Prague, Czech Republic, [4]Department of Physics, University of Texas at Dallas, Richardson, TX, USA, [5]British Antarctic Survey, Cambridge, UK

**Key Points:**
- Two distinct populations of plasmaspheric hiss are observed, one more field aligned and one more oblique, particularly at low L shells ($L < 3$)
- Oblique hiss is most prevalent during low geomagnetic activity levels and between 1900 and 0900 MLT-similar to oblique chorus waves
- Ray tracing confirms that oblique hiss at low L shells is in keeping with the existing theory of chorus as the source of plasmaspheric hiss

**Correspondence to:**
D. P. Hartley,
david-hartley@uiowa.edu

**Citation:**
Hartley, D. P., Kletzing, C. A., Santolík, O., Chen, L., & Horne, R. B. (2018). Statistical properties of plasmaspheric hiss from Van Allen Probes observations. *Journal of Geophysical Research: Space Physics*, *123*, 2605–2619. https://doi.org/10.1002/2017JA024593

Received 13 JUL 2017
Accepted 25 FEB 2018
Accepted article online 28 FEB 2018
Published online 12 APR 2018



**Abstract** Van Allen Probes observations are used to statistically investigate plasmaspheric hiss wave properties. This analysis shows that the wave normal direction of plasmaspheric hiss is predominantly field aligned at larger L shells, with a bimodal distribution, consisting of a near-field aligned and a highly oblique component, becoming apparent at lower L shells. Investigation of this oblique population reveals that it is most prevalent at $L < 3$, frequencies with $f/f_{ce} > 0.01$ (or $f > 700$ Hz), low geomagnetic activity levels, and between 1900 and 0900 magnetic local time. This structure is similar to that reported for oblique chorus waves in the equatorial region, perhaps suggesting a causal link between the two wave modes. Ray tracing results from HOTRAY confirm that it is feasible for these oblique chorus waves to be a source of the observed oblique plasmaspheric hiss population. The decrease in oblique plasmaspheric hiss occurrence rates during more elevated geomagnetic activity levels may be attributed to the increase in Landau resonant electrons causing oblique chorus waves to be more substantially damped outside of the plasmasphere. In turn, this restricts the amount of wave power that can access the plasmasphere and evolve into oblique plasmaspheric hiss. These results confirm that, despite the difference in location of this bimodal distribution compared to previous studies, a direct link between oblique equatorial chorus outside of the plasmasphere and oblique hiss at low L shells is plausible. As such, these results are in keeping with the existing theory of chorus as the source of plasmaspheric hiss.

## 1. Introduction

Plasmaspheric hiss is a whistler mode wave that is typically observed in the high-density regions of the plasmasphere (e.g., Dunckel & Helliwell, 1969; Russell et al., 1969; Thorne et al., 1973) or in plasmaspheric plumes (e.g., Chan & Holzer, 1976; Summers et al., 2008). Occurring at frequencies typically between 100 Hz and ~5 kHz, plasmaspheric hiss may be observed during all geomagnetic conditions, but has shown to intensify during periods of elevated geomagnetic activity (e.g., Meredith et al., 2004; Smith et al., 1974; Thorne et al., 1974, 1977). Plasmaspheric hiss has been shown to play an important role in driving particle dynamics in the inner magnetosphere, namely, pitch angle scattering of radiation belt electrons (e.g., Selesnick et al., 2003) resulting in a net depletion as particles temporarily populate the bounce loss cone and are subsequently lost to the atmosphere (e.g., Abel & Thorne, 1998). It is widely believed that this is the primary mechanism for causing the slot region between the inner and outer radiation belts (e.g., Lyons & Thorne, 1973; Lyons et al., 1972).

Several hypotheses have been proposed detailing the origins of plasmaspheric hiss. It has been demonstrated that amplification of an "embryonic" source within the plasmasphere (e.g., Solomon et al., 1988) does not typically provide sufficient wave growth to account for observed plasmaspheric hiss wave intensities (Church & Thorne, 1983; Huang et al., 1983). However, recent observations by Summers et al. (2014) have shown evidence that plasmaspheric hiss can in some cases occur as coherent emission with a complex fine structure of discrete rising and falling tone elements, supported by subsequent analysis (Nakamura et al., 2016; Omura et al., 2015) that the generation mechanism for plasmaspheric hiss could be explained by applying nonlinear wave growth theory (typically used for whistler mode chorus waves) in the region close to the magnetic equator just inside of the plasmapause. Lightning-generated whistlers developing into plasmaspheric hiss after multiple magnetospheric reflections (e.g., Draganov et al., 1992) have been shown to play a role only

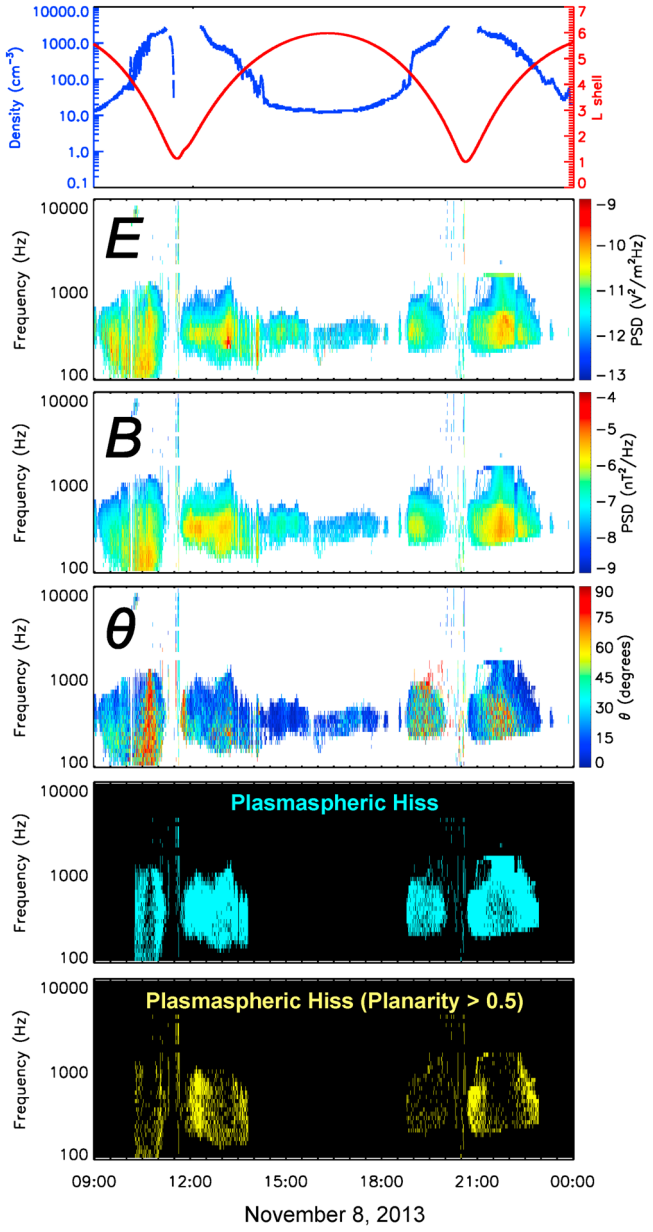


**Figure 1.** Overview of Van Allen Probe A observations from 8 November 2013; (top to bottom) plasma density (blue) and L shell (red), electric field power spectral density, magnetic field power spectral density, wave normal angle, plasmaspheric hiss wave flag (blue), and plasmaspheric hiss wave flag with additional planarity criterion (yellow).

for wave frequencies greater than ~2 kHz (Meredith et al., 2006). Another well-established theory is that plasmaspheric hiss originates from whistler mode chorus waves penetrating into the plasmasphere at high latitudes (e.g., Bortnik et al., 2008, 2009; Bortnik, Chen, Li, Thorne & Horne, 2011; Bortnik, Chen, Li, Thorne, Meredith, et al., 2011; Chum & Santolik, 2005; Li et al., 2015; Meredith et al., 2013; Santolík et al., 2006) from a source location close to the equatorial plane at higher L shell. This mechanism has been shown to be able to reproduce typical hiss wave power, frequency range, and spatial structure (Chen et al., 2012, 2012a, 2012b).

In this study, a statistical analysis of the plasmaspheric hiss wave properties is performed over a range of different L shells within the plasmasphere. Previous studies have reported both an approximately field-aligned, and a highly oblique, population of plasmaspheric hiss waves only at larger L shells within the plasmasphere (e.g., Hayakawa et al., 1986; Hayakawa & Sazhin, 1992; Storey et al., 1991), with predominantly field-aligned waves observed at L shells between 3.6 and 4.2 (e.g., Santolík et al., 2001). These results were consistent with the ray tracing simulations presented by Bortnik, Chen, Li, Thorne, Meredith, et al. (2011). This study reports that the population of more oblique plasmaspheric hiss waves is most prevalent at lower L shells, particularly $L < 3$. The properties of both the more field aligned and the more oblique wave populations are subsequently investigated as a function of frequency, magnetic local time (MLT), geomagnetic activity, and L shell. In addition, the HOTRAY ray tracing model (Horne, 1989) is used to offer an explanation of the origin of this oblique population of plasmaspheric hiss that is in keeping with current theory.

## 2. Instrument and Data Analysis

The Electric and Magnetic Field Instrument Suite and Integrated Science (EMFISIS) waves instrument (Kletzing et al., 2013) on board the Van Allen Probes twin satellite mission routinely collects survey measurements of the wave electric and wave magnetic fields with a half-second collection period occurring every 6 s. From this survey data, wave parameter summaries are generated. These include information detailing the total power of the wave electric and wave magnetic fields, the planarity and ellipticity (Santolík et al., 2003), and polarization (Santolík et al., 2002) of the waves, in addition to the wave normal angle determined via singular value decomposition (SVD) (Santolík et al., 2003). It is these parameters from the Van Allen Probes EMFISIS instrument, using all available data during the period between 1 October 2012 and 30 April 2016, that are implemented in the following analysis.

Prior to performing a statistical analysis on a specific wave mode (plasmaspheric hiss in this case), it is crucial to ensure that only waves of the desired type are included, with other wave modes rejected. This may be done by testing all observations against a rigorous selection criteria. In this study, for a wave to be identified as plasmaspheric hiss, the following criteria must be satisfied: (1) The spacecraft must be inside of the plasmasphere where the inner edge of the plasmapause is defined by a 100 $cm^3$ threshold, (2) The power spectral density in both the electric and magnetic field observations must be greater than 10 times the instrument background levels. (3) The degree of magnetic field polarization in the polarization plane (Santolík et al., 2002) and the ellipticity of the magnetic field polarization (Santolík et al., 2003) must be greater than 0.5 (ensuring that the wave polarization is coherent, near circular and right handed). This ellipticity criterion is imposed in order to ensure that magnetosonic waves, which are typically close to linear in polarization, are excluded from the statistical analysis. It is noted however that this does omit some cases of plasmaspheric hiss with oblique wave normal angles that occur with near-linear polarization, particularly at lower frequencies.

Relaxing this criterion to include waves with ellipticity values larger than 0.2 produces results extremely similar to those presented in this study, but with a higher chance of including some equatorial noise in the analysis. (4) The frequency range of the observed waves is between 100 Hz and 5 kHz. Additional data treatment includes removing periods of spacecraft charging, eclipse, boom shadow, and noisy frequency bands at ~2 and 4 kHz. It is noted that no correction is made to the electric field observations in order to account for antenna sheath impedance effects (e.g., Hartley et al., 2015, 2016, 2017).

Figure 1 provides an overview of wave observations from Van Allen Probe A on 8 November 2013, displaying (top to bottom) L shell (red) and plasma density (blue) determined from the upper hybrid line (Kurth et al., 2015), the total power of the wave electric, and wave magnetic, field where observations exceed 10 times instrument background levels, the wave normal angle, in addition to an indicator of the times and frequencies where the criteria for classifying the observed waves as plasmaspheric hiss are met (blue). However, in order to perform a statistical analysis on the wave normal directions, an additional defining criterion must also be imposed.

## 3. Planarity Limitation

The wave planarity (Santolík et al., 2003) is derived from the ratio of the smallest axis of the 3-D magnetic field polarization ellipsoid to its largest axis, therefore providing information as to the accuracy of the plane wave approximation. The planarity is obtained by subtracting this ratio from one; therefore, values near unity imply that the plane wave approximation is valid, and values much less than unity indicate that a significant fraction of the wave power exists outside of the polarization plane. If only a single plane wave is present, the planarity will be exactly one. In order to perform a statistical analysis on the wave normal angles of plasmaspheric hiss, it is crucial to impose a lower limit on the planarity of the waves included. This is due to the fact that the SVD method of determining wave normal directions is reliant on the plane wave approximation (assumption of a single plane wave). While SVD has been shown to provide reasonable results when the planarity is somewhat less than unity, this technique does not provide valid outputs in cases where the plane wave approximation breaks down (planarity $\ll 1$), yet an answer is provided regardless. It is therefore important to apply a planarity filter in order to ensure the validity of the technique, and therefore the validity of the results. Unfortunately, the planarity of plasmaspheric hiss can often be low (waves are broadband and incoherent), and as such, imposing a lower limit on the planarity can place limitations on the amount of data included in a statistical study. Here we impose a lower limit on the planarity of plasmaspheric hiss of 0.5, allowing for no more than 25% of power out of the polarization plane with respect to the power of the largest axis of the 3-D magnetic field polarization ellipsoid ($w_1/w_3 < 0.25$), where $w_1$, $w_2$, and $w_3$ are the three singular values output from the SVD analysis ordered into an ascending series. The percentage of the total power permitted outside of the polarization plane, $100\% \times w_1/(w_1 + w_2 + w_3)$, also depends on the wave ellipticity, since this provides information on the relationship between $w_2$ and $w_3$. A general expression for the percentage of total power outside of the polarization plane is $100\%/([(1 + Lp)/(1 - F)^2] + 1)$; where $Lp$ is ellipticity = $w2/w3$, and $F$ is planarity = $1 - \sqrt{w1/w3}$. It should be noted that this expression is not valid for all $Lp$ and $F$ values, since some $Lp$ values are not permitted for given values of $F$, and vice versa. Given the threshold values used in this study, $Lp > 0.5$, $F > 0.5$, this gives a maximum of 14% of total power outside of the polarization plane $w_1/(w_1 + w_2 + w_3) < 0.14$.

Figure 2 (left) shows the percentage of data included in this study after this criterion is imposed as a function of frequency. Note that this comparison is done after all other selection criteria have been imposed. At frequencies around 100 Hz, the planarity is greater than 0.5 in more than 50% of the cases. This reduces to around 40% between ~400 Hz and 2 kHz before increasing back to above 50% at higher frequencies. For completeness, the probability distribution function (PDF) (normalized occurrences in each frequency channel) of the wave planarity at each frequency is also shown in Figure 2 (right), with the lower planarity threshold of 0.5 indicated by the thick black line. The gaps at specific frequencies are due to the removal of frequency band with elevated noise levels. Figure 1 (bottom) shows how this additional criterion affects the classification of plasmaspheric hiss waves on 8 November 2013. Also provided in Figure 2 (bottom) is a table detailing the percentage of the total power permitted outside of the polarization plane for different planarity and ellipticity thresholds, with the thresholds used in this study highlighted in yellow.

It must be noted that the SVD method (as well as all other methods that assume the presence of a single plane wave) may often give false results for plasmaspheric hiss because its wave field is complex, with wave

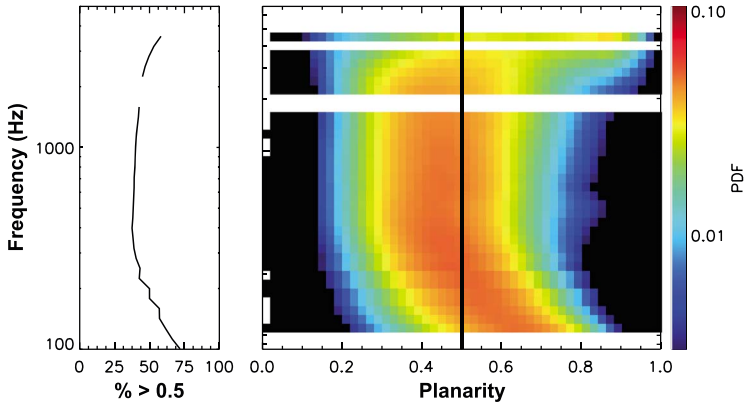


| | | | | | | | | |
|---|---|---|---|---|---|---|---|---|
| **Planarity Threshold** | > 0.7 | > 0.7 | > 0.5 | > 0.5 | > 0.3 | > 0.3 | > 0.2 | No Threshold |
| **Ellipticity Threshold** | > 0.7 | > 0.5 | > 0.7 | > 0.5 | > 0.7 | > 0.5 | > 0.7 | No Threshold |
| **% of Total Power Permitted Outside of Polarization Plane** | < 5% | < 6% | < 13% | < 14% | < 22% | < 25% | < 27% | < 33% Isotropic Noise |

**Figure 2.** (left) The percentage of waves identified as plasmaspheric hiss that meet the planarity > 0.5 threshold employed in this study. (right) Probability distribution function of the planarity of waves identified as plasmaspheric hiss, with the lower planarity threshold of 0.5 shown by the vertical black line. (bottom) Table detailing the maximum percentage of the total power permitted outside of the polarization plane for different planarity and ellipticity thresholds.

power spread in large theta intervals. This is highlighted by the fraction of cases where the planarity criterion is met in our study (Figure 2). The relationship between planarity and wave normal angle has also been investigated. In general, higher planarity values are observed for either near field-aligned or highly oblique waves. For wave normal angles in-between (~10° to ~60°), lower planarity values are typically obtained (figure not shown). For these cases, both near field-aligned and oblique wave vectors may be present at the same time, with SVD wave normal angle estimates yielding a weighted average of this more complex wave field. In placing a lower bound on the planarity, the impact that wave power from outside of the polarization plane can have on the weighted average of the wave normal angle determined through SVD can be minimized. For the low-planarity cases, wave distribution function (WDF) methods would be required in order to resolve the more complex wave field which may consist of a superposition of a distribution of different plane waves at the same frequency and time instance. WDF methods have been used to investigate plasmaspheric hiss (e.g., Santolík et al., 2001) with results showing that hiss often propagates parallel and antiparallel to the Earth's magnetic field, albeit with some power found at highly inclined wave normal directions, near the Gendrin angle. In order to keep the results of this study in context, it should be kept in mind during the subsequent analysis that only the subpopulation of plasmaspheric hiss waves that meet this planarity criterion can be studied using SVD methods.

It should also be noted that the lower planarity thresholds that have been employed in other studies give rise to the potential for nonphysical wave normal angles (determined assuming the presence of a single plane wave) to dominate statistical results, particularly given the occurrence rates of plasmaspheric hiss with low planarity as shown in Figure 2.

## 4. Statistical Results and Discussion

Having correctly isolated plasmaspheric hiss waves with well-defined wave normal directions, it is now possible to investigate this comprehensive data set.

Initially, the distribution of plasmaspheric hiss wave normal angles is investigated as a function of L shell and frequency. Figure 3 displays plasmaspheric hiss PDFs (number of occurrences normalized to the total number of occurrences for each frequency channel, where an occurrence is defined as any time instant, from the 6 s

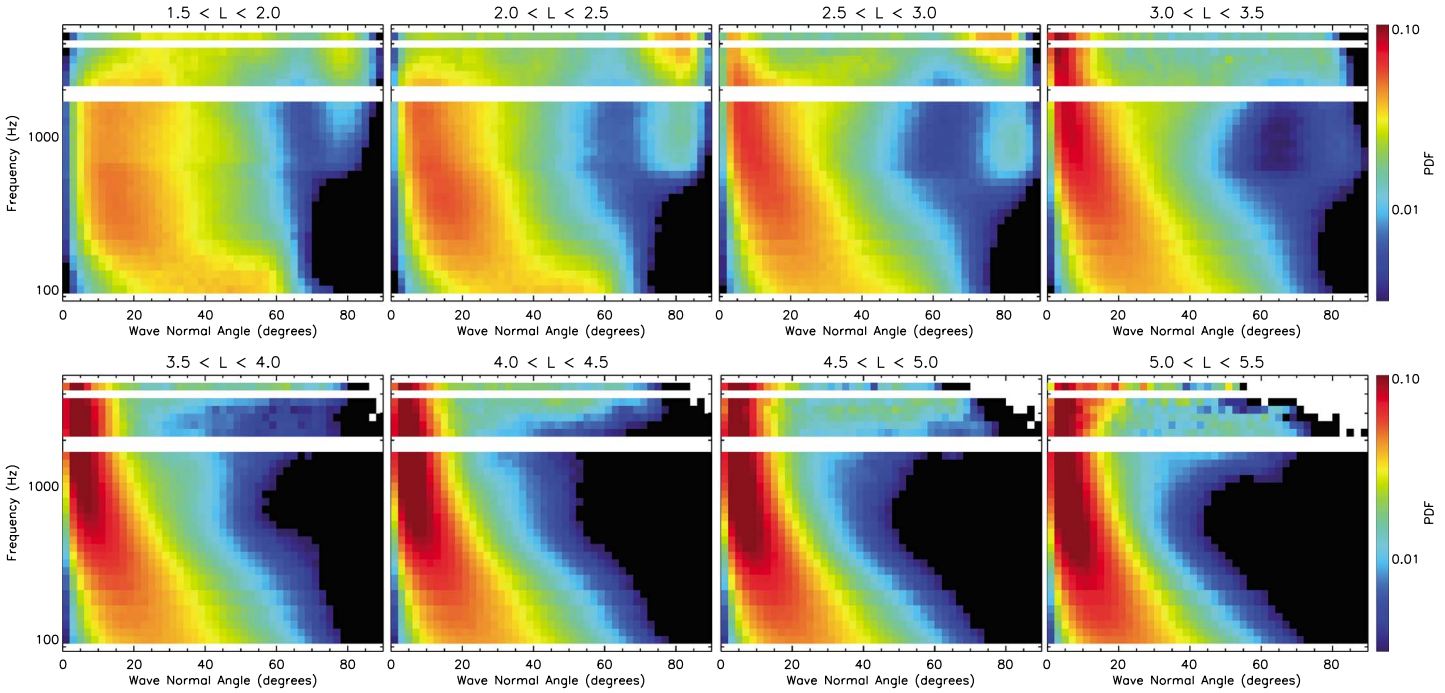


**Figure 3.** Probability distribution functions of the wave normal angle as a function of frequency in 0.5 L shell intervals from 1.5 to 5.5.

survey observations, where a wave is identified as hiss) for intervals of 0.5 in L shell ranging from 1.5 to 5.5. At lower L shell intervals, two distinct populations of plasmaspheric hiss are observable; one that is more aligned with the background magnetic field direction (referred to as the primary population hereafter), and one with more oblique wave normal directions (referred to as the secondary population hereafter). In contrast, at higher L shells this secondary population is no longer apparent with the wave normal angle predominantly field aligned. It is also apparent that the primary wave population spans the entire plasmaspheric hiss frequency range (100 Hz to 5 kHz), whereas the secondary population is only really apparent at frequencies greater than 700 Hz.

The distribution of plasmaspheric hiss waves is investigated at L shells less than 3.0 in order to better parameterize these two distinct populations. Figure 4 shows the number of occurrences, *N*, the probability distribution function, PDF, the cumulative power spectral density of the electric field, $\boldsymbol{E}$ ($V^2\ m^{-2}\ Hz^{-1}$), and the cumulative power spectral density of the magnetic field, $\boldsymbol{B}$ ($nT^2\ Hz^{-1}$), as a function of frequency and wave normal angle for L shells less than 3.0. Cumulative power spectral densities are defined as the power spectral density binned in intervals of frequency and wave normal angle before being summed over all time instances where waves are identified as plasmaspheric hiss. Note that this figure is in the same format as presented for chorus waves in Li et al. (2016) in order to permit simple comparisons. The two-population structure is evident in both the plot showing the number of occurrences and the plot showing the PDF. The primary population occurs at wave normal angles less than ~50–60° and the secondary population occurs at wave normal angles greater than ~70°. Waves in the primary population are shown to contain significant power in both the electric and magnetic fields, whereas waves in the secondary population contain a stronger electric field and a weaker magnetic field. This result is similar to that presented for chorus waves by Li et al. (2016), with the primary population being quasi-parallel and the secondary oblique population being quasi-electrostatic, as is typical for whistler mode emissions.

While the statistical results presented in Figure 4 provide some insight into these two populations, some questions remain: Do the propagation angles of the more oblique waves relate to the Gendrin angle (Gendrin, 1961) or the resonance cone angle? Are there specific locations in MLT or specific geomagnetic activity levels that cause these more oblique waves to occur? In order to address these questions, Figure 4 is reproduced as a function of frequency normalized to the value of the local electron cyclotron frequency ($f/f_{ce}$). This allows for both the Gendrin angle ($\cos\theta_G = (2f/f_{ce})$) and the high-density approximation of the resonance cone angle ($\cos\theta_{res} = f/f_{ce}$) to be easily overplotted. This is shown in Figure 5 with the solid black line representing

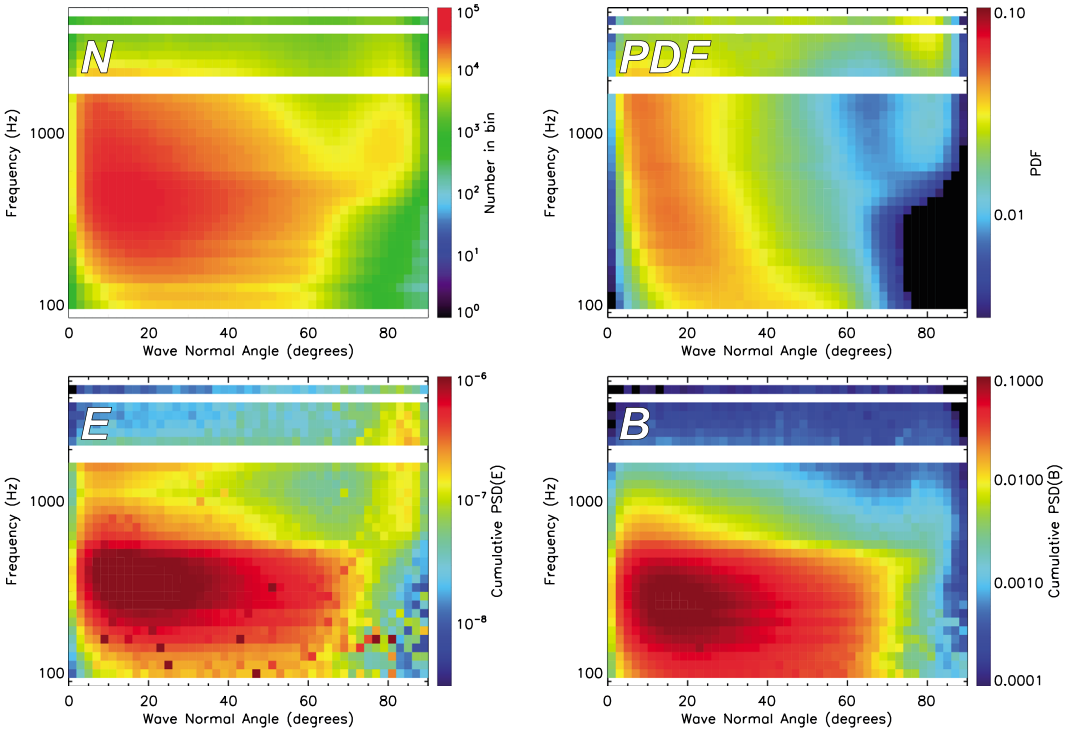


**Figure 4.** Number of occurrences, *N*, probability distribution function, PDF, cumulative electric field power spectral density, ***E*** ($V^2\ m^{-2}\ Hz^{-1}$), and the cumulative magnetic field power spectral density, ***B*** ($nT^2\ Hz^{-1}$), as a function of frequency and wave normal angle for L shells less than 3.0.

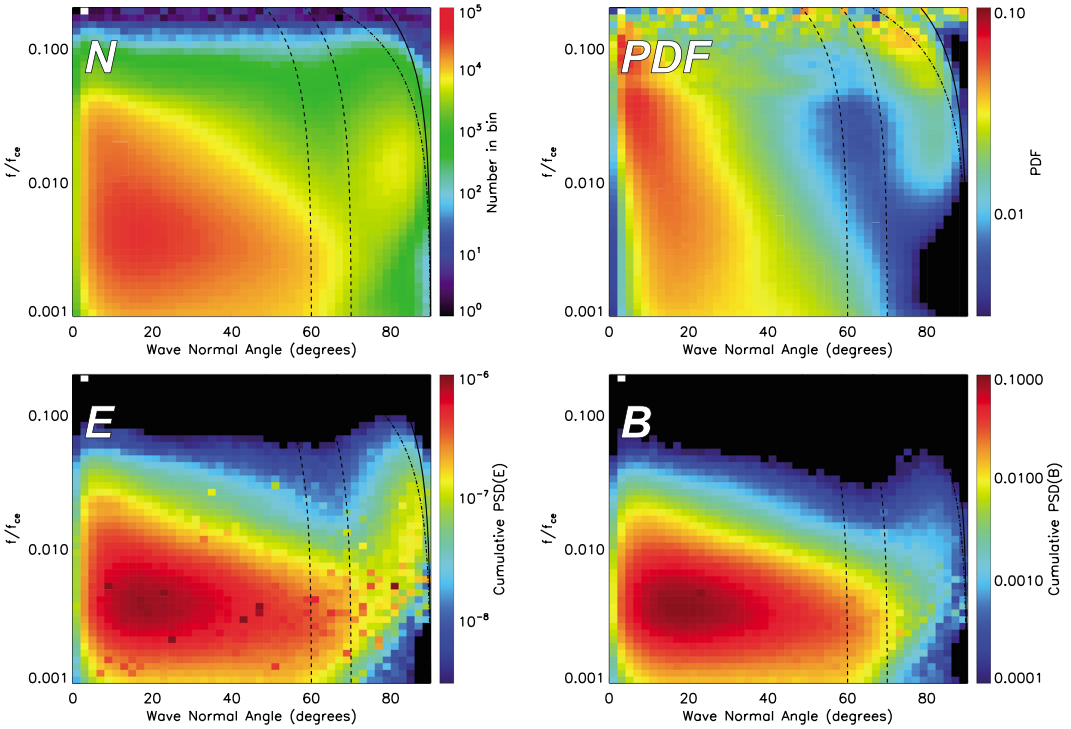


**Figure 5.** Number of occurrences, *N*, probability distribution function, PDF, cumulative electric field power spectral density, ***E*** ($V^2\ m^{-2}\ Hz^{-1}$), and the cumulative magnetic field power spectral density, ***B*** ($nT^2\ Hz^{-1}$), as a function of frequency normalized to the electron cyclotron frequency and wave normal angle for L shells less than 3.0. The resonance cone angle (solid), Gendrin angle (dash-dotted), and separation angles employed in this study (dashed) are overplotted in black.

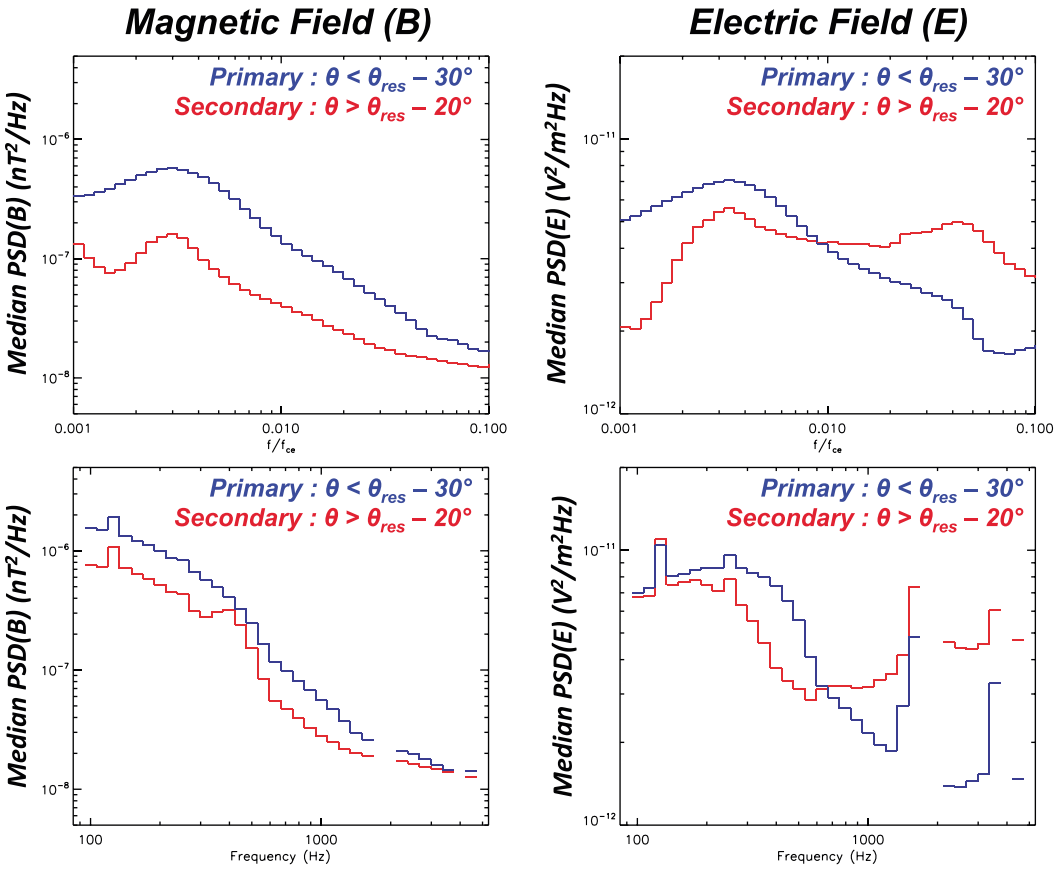


**Figure 6.** Median (left) magnetic ($nT^2$ $Hz^{-1}$) and (right) electric ($V^2$ $m^{-2}$ $Hz^{-1}$) field power spectra of the primary (blue) and secondary (red) plasmaspheric hiss wave populations as a function of $f/f_{ce}$ (top) and frequency (bottom).

the resonance cone angle and the dash-dotted line representing the Gendrin angle. Showing the data in this way reveals that the secondary population occurs relatively close to the Gendrin angle, a feature that is particularly apparent in the panel showing the PDF. However, across the majority of the frequency range of plasmaspheric hiss, there is very little difference between the Gendrin angle and the resonance cone angle, making it difficult to establish if these obliquely propagating waves are particularly well associated with either angle. It should also be noted again that the primary wave population spans the entire plasmaspheric hiss frequency range, whereas the secondary wave population only occurs at frequencies with $f/f_{ce}$ greater than 0.01 (compared to >700 Hz when plotted as a function of frequency).

Before performing in-depth comparisons of the two wave populations, it is necessary to generate criteria to separate them. Through simple visual inspection, it is apparent that the secondary wave population is relatively well contained within 20° of the resonance cone angle ($\theta_{res} - 20° < \theta_k < \theta_{res}$), whereas the primary wave population is typically confined to smaller angles that are greater than 30° away from the resonance cone angle ($\theta_k < \theta_{res} - 30°$). These two separation angles of $\theta_{res} - 30°$ and $\theta_{res} - 20°$ are shown by the dashed black lines in Figure 5. This criterion is used to distinguish between the two different wave populations in the subsequent analysis.

Initially, the electric and magnetic field wave power spectra are directly compared for the two plasmaspheric hiss wave populations. Figure 6 shows the median power spectral density of the magnetic (left) and electric (right) fields as a function of frequency normalized to the local cyclotron frequency, $f/f_{ce}$, (top) and frequency (bottom) for both the primary wave population (blue) and the secondary wave population (red). Note that some slightly noisy frequency bands remain visible in the electric field data when plotted as a function of frequency. For the magnetic field power spectra, both populations exhibit a similar shape, albeit with the magnitude of the secondary wave population lower than that of the primary population. Both populations exhibit a peak in their power spectra between 0.003 and $0.004 f/f_{ce}$ (around 100 Hz in frequency),

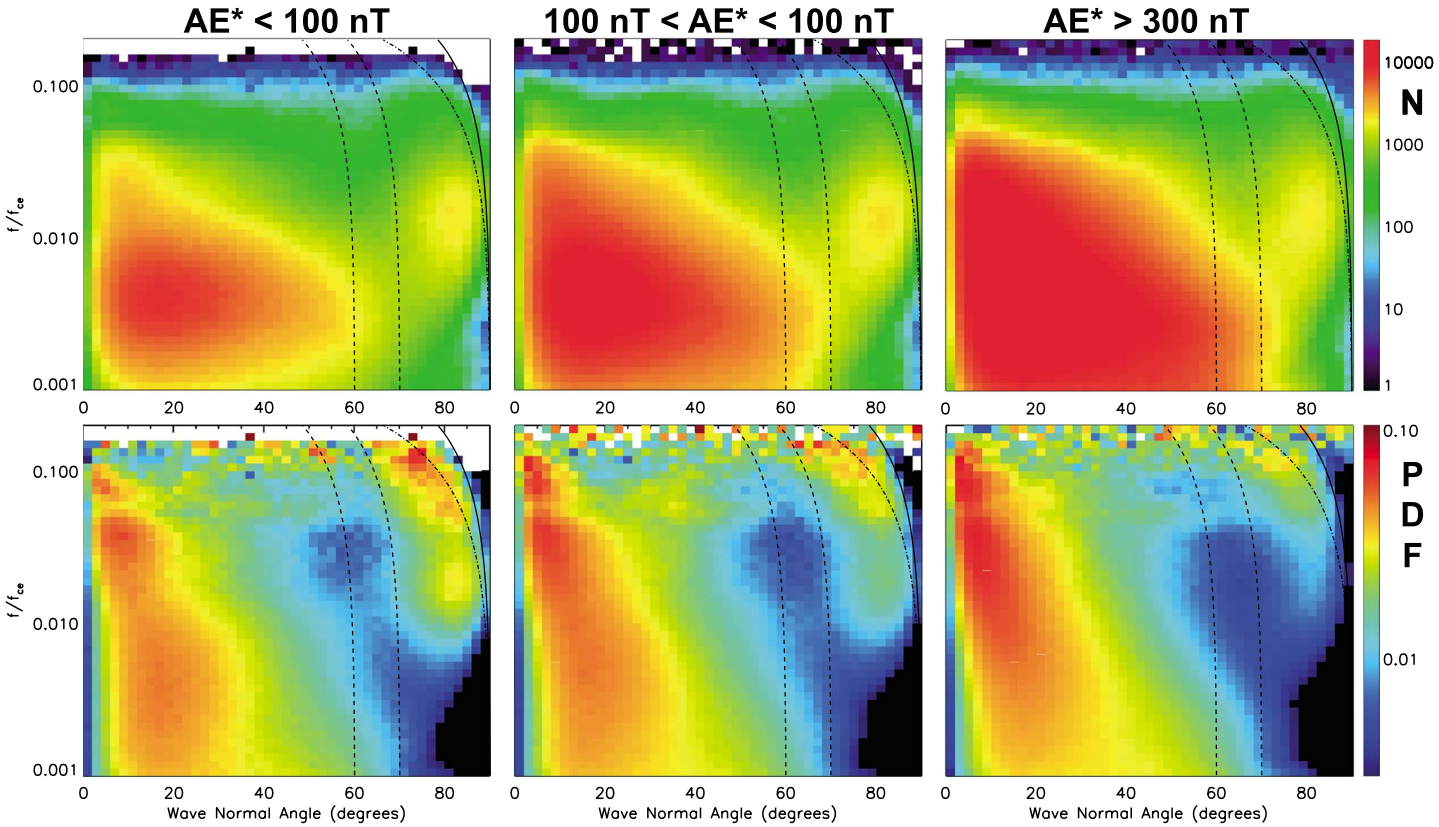


**Figure 7.** Number of occurrences, *N*, and probability distribution function, PDF, as a function of normalized frequency and wave normal angle at $L < 3.0$ for three different geomagnetic activity levels.

with their power spectral densities reducing at higher frequencies. In comparison, the primary and secondary wave populations display differently shaped electric field power spectra. The primary wave population peaks between 0.003 and $0.004 f/f_{ce}$, similar to the magnetic field, before reducing with increasing frequency. There is, perhaps, a hint at a secondary peak around $0.004 f/f_{ce}$, but this appears more as a temporary flattening of the distribution before reducing further at higher frequencies. This is likely caused by the noisy frequency bands that occur close to ~2 and 4 kHz. For the secondary wave population, a double peak is certainly evident with local maxima in power spectral density occurring at $0.003–0.004 f/f_{ce}$ and $0.04–0.05 f/f_{ce}$ that are approximately equal in magnitude. At frequencies with $f/f_{ce}$ less than 0.01 (or 700 Hz in frequency) the magnitude of the electric field power spectral density is greater for the primary wave population. Conversely, at frequencies with $f/f_{ce}$ greater than 0.01 (or 700 Hz in frequency) the magnitude of the electric field power spectral density is greater for the secondary wave population.

Having identified differences in the electric and magnetic field power spectra of the primary and secondary plasmaspheric hiss wave populations, these two populations are further investigated as a function of MLT and geomagnetic activity.

Figure 7 displays the number of occurrences, *N*, and the probability distribution function, PDF, as a function of normalized frequency and wave normal angle for L shells less than 3.0 for three different geomagnetic activity levels as indicated by the AE* index (highest recorded AE index in the preceding 3 h period). These geomagnetic activity levels are defined as low activity (AE* < 100 nT), moderate activity (100 nT < AE* < 300 nT), and high activity (AE* > 300 nT). As with Figure 5, the resonance cone angle, the Gendrin angle, as well as the two separation angles used in this study are shown by black solid, dash-dotted, and dashed lines, respectively. Showing data in this way allows for the occurrence rates of the primary and secondary plasmaspheric hiss populations to be easily compared against each other and to observe their relative variability as a function of geomagnetic activity. It is apparent from Figure 7 that the highest probability of observing waves in the secondary

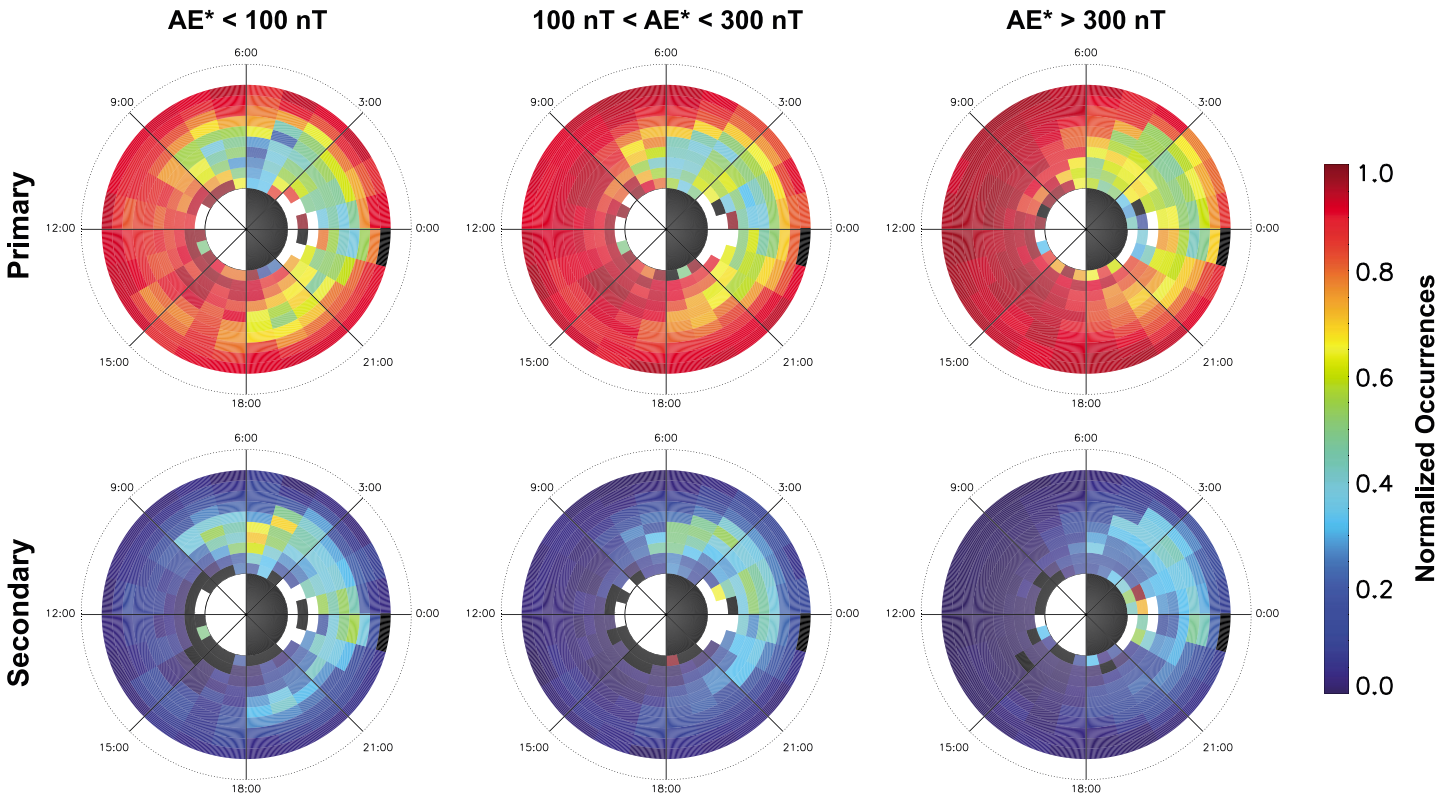


**Figure 8.** Normalized occurrence rates of the primary (top) and secondary (bottom) plasmaspheric hiss wave populations as a function of geomagnetic activity, magnetic local time, and L shell.

population occurs during low geomagnetic activity, with the likelihood of observing waves from the secondary population decreasing with increasing geomagnetic activity as the primary population becomes more dominant.

Figure 8 shows the MLT and L shell variation of the normalized occurrence rates of the primary and secondary wave populations for normalized frequencies with $f/f_{ce}$ greater than 0.01, for three different geomagnetic activity levels as indicated by the AE* index. It should be noted that using a lower-frequency bound of 700 Hz, instead of $0.01f/f_{ce}$, produces nearly identical figures. It should also be noted that using the lower hybrid frequency normalized to the electron cyclotron frequency ($f_{LH}/f_{ce} \sim 0.023$) could be used as a physical parameter to delineate observations (since this frequency dictates the boundary between where the resonance cone angle does and does not exist). However, it can be seen in Figure 5 that a substantial part of the oblique population does exist below this frequency boundary, as such, $0.01f/f_{ce}$ is used hereafter. From Figure 8, it is again evident that the highest probability of observing waves in the secondary population occurs during low geomagnetic activity and decreases as geomagnetic activity increases. It is also apparent that it is not just the occurrence rates that decrease with increasing geomagnetic activity but also the range of magnetic local times where oblique waves are observed. During low geomagnetic activity, oblique plasmaspheric hiss waves are observed at low L shells between ~19:00 and ~9:00 MLT with typical occurrence rates in this region of ~40%. The size of this region reduces slightly during moderate geomagnetic activity, with occurrence rates decreasing somewhat between ~19:00 and ~21:00 MLT. During high geomagnetic activity, the region of oblique plasmaspheric hiss waves is smaller still, typically confined between ~19:00 and ~5:00 MLT.

These results differ from those of Yu et al. (2017) who reported that the wave normal angle of plasmaspheric hiss in most regions did not depend strongly on substorm activity. The exception to this was an increase in wave normal angles in the nightside at low L shells during more intense substorm activity. However, it should be noted that this study used a lower planarity threshold than is employed in the current study (0.2 as opposed to 0.5) to define plasmaspheric hiss. This may, in some cases, give rise to the potential for including nonphysical wave normal angles (determined via SVD) as discussed in section 3.

The variation of oblique plasmaspheric hiss wave occurrence rates with MLT (Figure 8) appears remarkably similar to the structure observed for oblique chorus waves by Li et al. (2016), although notably at different L shell ranges. This, perhaps, suggests a causal link between the two obliquely propagating wave modes. It has been noted by numerous authors (e.g., Bortnik et al., 2008, 2009; Chum & Santolik, 2005; Li et al., 2015; Meredith et al., 2013; Santolík et al., 2006) that chorus waves can penetrate into the plasmasphere and evolve into plasmaspheric hiss. A ray tracing simulation study performed by Bortnik, Chen, Li, Thorne, Meredith, et al., (2011) reported a bimodal distribution of wave normal angles, containing a more field-aligned and a highly oblique component, particularly at larger L shells close to the plasmapause. However, with the new results indicating that a bimodal distribution of wave normal angles is apparent only deep inside of the plasmasphere, we perform a preliminary investigation to see whether the occurrence of oblique hiss at low L shells is in keeping with the existing theory of chorus as the source of plasmaspheric hiss.

## 5. Ray Tracing (HOTRAY)

In order to test the plausibility of oblique chorus waves entering the plasmasphere and evolving into oblique plasmaspheric hiss at low L shells, the HOTRAY (Horne, 1989) ray tracing program is implemented. To fully assess the gain/damping rates along the wave trajectories, it is required to model particle distributions based on spacecraft observations, allowing for the suprathermal electron distribution to be quantified. However, we initially implement a cold plasma density model in order to provide a test of the plausibility of oblique chorus waves entering the plasmasphere and evolving into oblique plasmaspheric hiss. While path-integrated gains are not explicitly calculated for this initial test of plausibility, it may be assumed that waves with larger wave normal angles are generally shorter lived than waves with more parallel wave normal directions in similar plasma mediums.

It has been shown (e.g., Bortnik et al., 2008, 2009; Bortnik, Chen, Li, Thorne & Horne, 2011; Bortnik, Chen, Li, Thorne, Meredith, et al., 2011; Chen et al., 2012, 2012a, 2012b) that chorus waves with initial wave normal angles ~40–65° launched at $L = 6$ in the equatorial plane can gain access to the plasmasphere. Such waves typically experience damping outside of the plasmasphere, but once inside the plasmasphere the Landau damping rates are much weaker due to the difference in the suprathermal electron distribution (e.g., Li et al., 2010). It is noted that the following ray tracing simulations are by no means exhaustive. Previous works have shown the propagation of chorus waves into the plasmasphere and subsequent evolution into plasmaspheric hiss, with more comprehensive ray tracing simulations by varying initial angle of propagation, source location, and wave frequency. These studies (Bortnik, Chen, Li, Thorne, & Horne, 2011; Bortnik, Chen, Li, Thorne, Meredith, et al., 2011; Bortnik et al., 2016; Chen et al., 2012, 2012a, 2012b) were able to reproduce a wave power, frequency range, and spatial structure consistent with previous observational results. That is, a field-aligned population over a broad range of L shells, with an oblique component apparent only in the outer plasmasphere (bimodal distribution). However, the statistical results presented here provide a contrasting picture, with the oblique population of plasmaspheric hiss apparent only in the inner plasmasphere, particularly inside $L = 3$. The ray tracing results presented here are intended as an initial test to see whether the occurrence of oblique hiss at low L shells is in keeping with the existing theory of chorus as the source of plasmaspheric hiss.

Figure 9 shows an example ray, launched in the equatorial plane at 6 $R_E$ with an initial wave normal angle of −54° and a frequency of ~1 kHz (0.25 $f/f_{ce}$ at 6 $R_E$ ) with colors used to highlight the temporal evolution. Also shown is the modeled equatorial density profile (diffusive equilibrium), the wave normal angle (with the resonance cone shaded in gray), the L shell at each point that the wave trajectory crosses the equatorial plane, the latitude of the wave trajectory, and the wave frequency normalized to the value of the local electron cyclotron frequency. The wave normal angle of this wave decreases to zero as it propagates to high latitudes outside of the plasmasphere (consistent with experimental results of Santolík et al., 2014). The wave then enters the plasmasphere close to the Earth at high latitude before performing multiple magnetospheric reflections as it propagates outward to higher L. Once the wave reaches a certain radial distance (~3.5 $R_E$ in this case), it remains approximately fixed at the same L shell for many traversals. Crucial to the analysis presented here, the wave normal angle remains very oblique (close to the resonance cone) once the wave is inside of the plasmasphere. Following the assumption that waves with large wave normal angles would damp away, it is assumed that the power of such a wave would steadily decrease over the ray path once it has entered the plasmasphere. The result of this would be that waves of this type would be most readily observed at low L

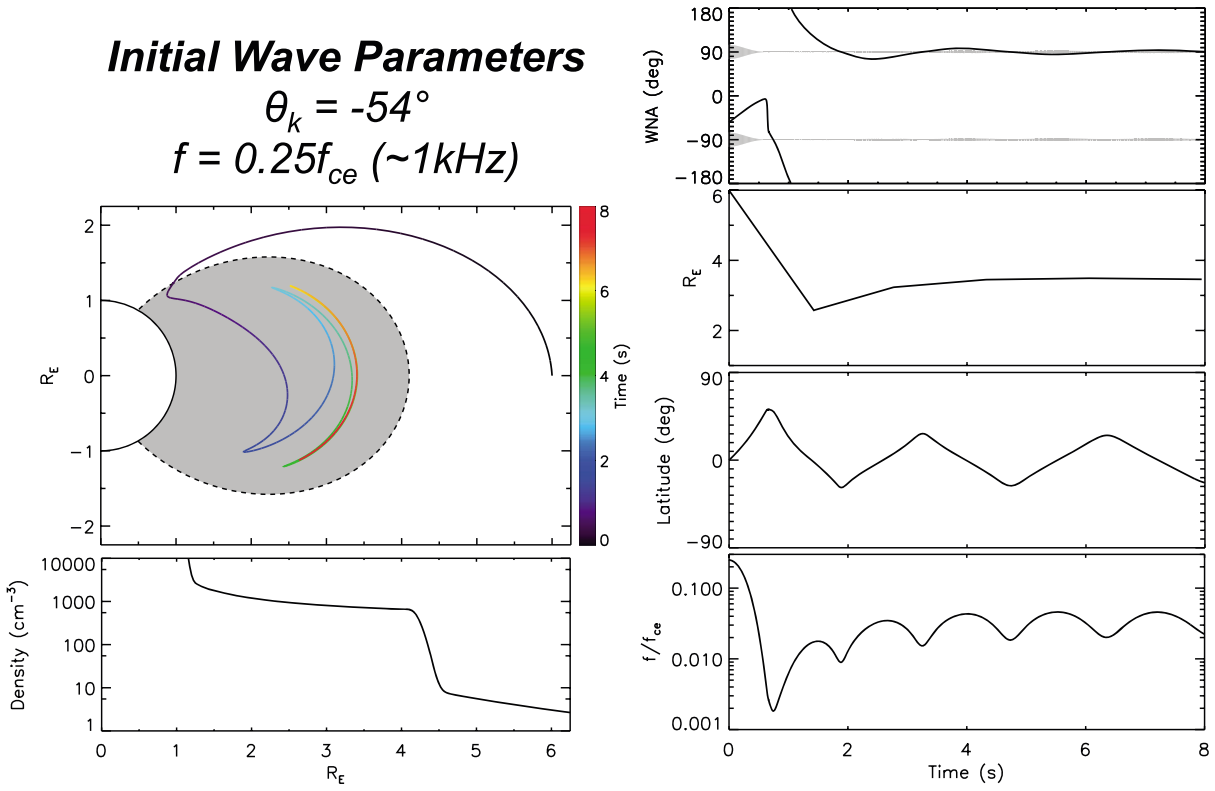


**Figure 9.** Trajectory of a ray launched at 6 $R_E$, $\theta = -54°$, and $f = 0.25f/f_{ce}$ (~1 kHz). The modeled equatorial density profile, evolution of the wave normal angle, the L shell at each crossing of the equatorial plane, the latitude of the wave trajectory, and the normalized wave frequency are also shown.

shells and as the wave propagates outward in L and damps away, the wave power would drop below the 10 times background levels threshold employed in this study. It is noted that the initial wave frequency and wave normal direction are consistent with oblique lower band chorus waves in their equatorial generation region outside of the plasmasphere. Furthermore, once the wave is inside of the plasmasphere, the wave frequency is between 0.01 and 0.05 $f/f_{ce}$, which is consistent with the frequency range where oblique hiss waves are observed in the Van Allen Probes data as shown in Figure 5.

With initial ray tracing results demonstrating that it is plausible for oblique chorus to propagate into the plasmasphere and be observed as oblique plasmaspheric hiss at low L shells, we now perform a more detailed ray tracing analysis using multiple rays with explicitly calculated damping rates. In order to calculate growth/damping rates, we implement a modeled suprathermal electron distribution (100 eV to a few keV) derived from measurements from the Time History of Events and Macroscale Interactions during Substorms (THEMIS) spacecraft (varying with L, MLT, and geomagnetic activity) in addition to the cold electron density model (details may be found in Chen et al., 2012a, 2012b).

First, a full range of wave normal angles (0° to −90°) is traced with a relatively coarse initial wave normal angle grid (2° intervals). The wave frequency is set to 1 kHz, with the launch position located in the equatorial plane at 6 $R_E$ and MLT = 4 (where oblique hiss is frequently observed in the statistical results). From this preliminary ray tracing, a subset of wave normal angles that gain access to the plasmasphere under the simulated conditions is obtained. This allows for both the range of, and interval between, initial wave normal angles to be reduced (smaller, finer grid), and for us to really focus on the waves that gain access to the plasmasphere. Figure 10 (top) shows the propagation of this subset of waves with initial wave normal angles varying from −40° (blue) to −60° (red) in intervals of 0.5°. Also shown is the path-integrated gain/damping (middle) and the wave normal angle evolution (bottom) of each wave trajectory. Each column of the figure displays these parameters for a different level of geomagnetic activity; low activity (AE* < 100 nT, left), moderate activity (100 nT < AE* < 300 nT, middle), and high activity (AE* >300 nT, right). Waves that drop below a path-integrated damping threshold of −30 dB are considered to be fully damped and are no longer traced. It is evident from this figure that damping rates outside of the plasmasphere increase with increasing

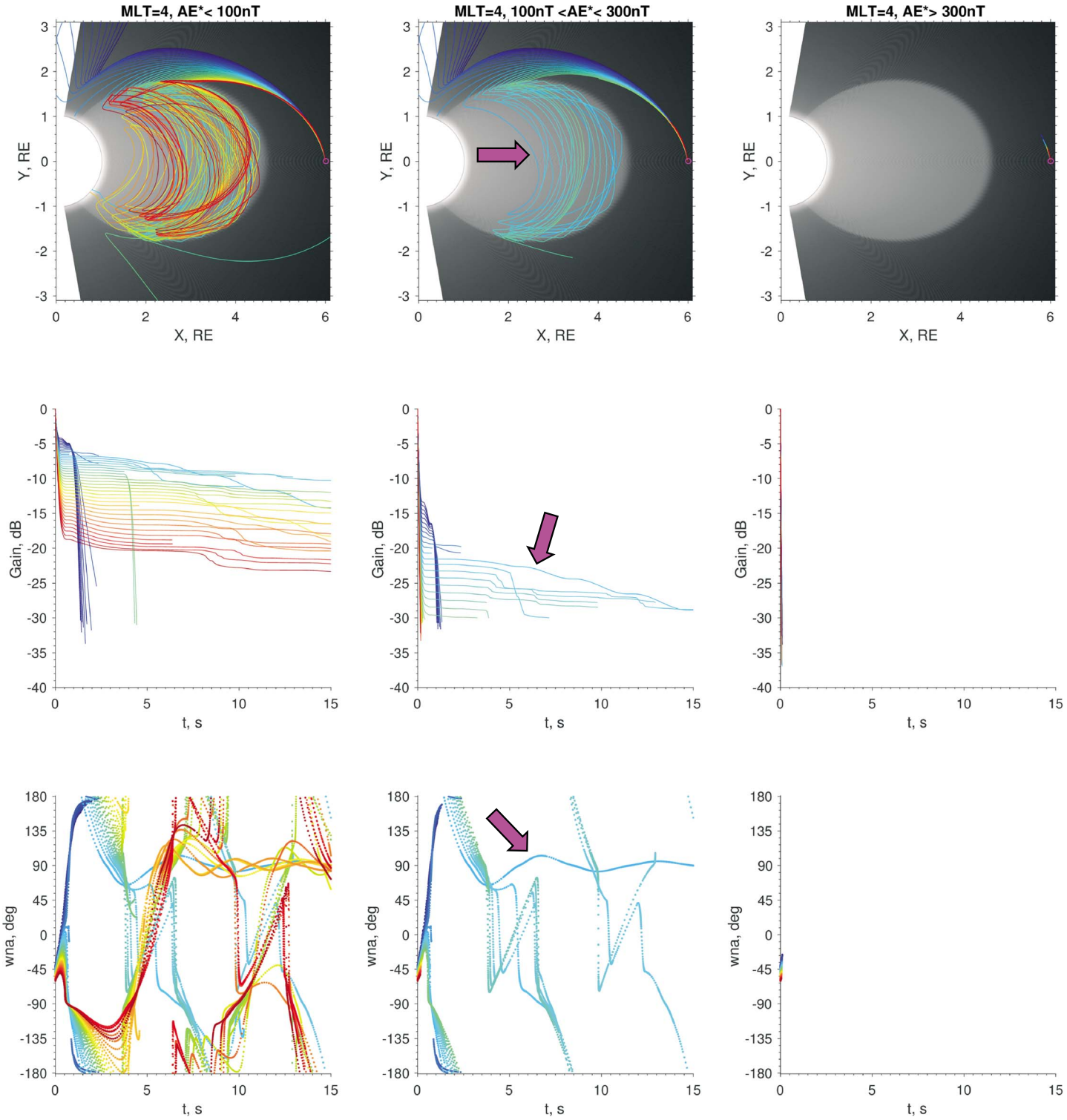


**Figure 10.** Ray trajectories (top), path-integrated gain/damping (middle), and wave normal angle evolution (bottom) of 1 kHz waves, launched at 6 $R_E$ and MLT = 4 with initial wave normal angles varying from −40° (blue) to −60° (red) in intervals of 0.5° for low (left), moderate (middle), and high (right) geomagnetic activity levels as indicated by AE*.

geomagnetic activity, with many ray paths entering the plasmasphere with sufficient power during low geomagnetic activity and no rays with sufficient power entering the plasmasphere during the highest levels of geomagnetic activity. This is due to the increase in low-energy Landau resonant electrons associated with an elevated AE* index (which is a proxy for substorm activity) leading to stronger Landau damping outside of the plasmasphere. Hence, due to increased Landau damping during elevated activity, fewer waves are able to penetrate into the plasmasphere and be observed as oblique plasmaspheric hiss at low L shells, a picture consistent with the structure observed in the statistics from Van Allen Probes in Figures 7 and 8. Another key feature is that of the waves that do propagate into the plasmasphere, it is the waves with initial wave normal angles between −45° and −50° (least oblique of the waves that enter the plasmasphere) that propagate to the lowest L shells, become highly oblique, and actually experience the slowest damping rates. This is perhaps most apparent (due to the limited number of rays) for the wave path highlighted by the pink arrow in Figure 10 (but is also apparent for low geomagnetic activity with even slower damping rates). This is again consistent with the result that oblique plasmaspheric hiss, caused by oblique chorus, would be most readily observed at low L shells with the wave power likely to drop below the 10 times instrument background levels threshold employed in this study as the wave propagates outward to higher L.

It is worth noting that ray tracing results can vary significantly depending on the source location of the oblique chorus waves, the implementation of different density profiles and structures, or by varying the suprathermal electron distribution with geomagnetic activity (as shown in Figure 10). However, under the conditions presented in this study, it has been demonstrated that this picture of initially oblique chorus waves propagating quasi-parallel at higher latitudes, penetrating into the plasmasphere and creating oblique plasmaspheric hiss at low L shells, particularly during low geomagnetic activity, is both plausible and consistent with what is observed statistically in the Van Allen Probes observations.

The ray tracing results presented here demonstrate that it is feasible for initially oblique equatorial chorus to propagate into the plasmasphere and be observed with significant power as oblique hiss in the inner plasmasphere (gain > −30 dB). As such, the occurrence of oblique hiss at low L shells is in keeping with the existing theory of chorus as the source of plasmaspheric hiss (both field-aligned and oblique). These ray tracing results provide an initial test of plausibility only. In order to establish if ray tracing simulations can fully reproduce the new statistical results from the Van Allen Probes of oblique hiss at low L shells (rather than in the outer plasmasphere as reported in previous studies), a more thorough and complete ray tracing study would be required. This is beyond the scope of the current analysis.

## 6. Conclusions

This study has evaluated the wave normal distribution of plasmaspheric hiss waves using observations from the Van Allen Probes satellite mission. It has been found that two populations of plasmaspheric hiss exist; a primary approximately field-aligned population, and a secondary more oblique population that is most prevalent inside $L = 3$. This is in contrast to the results of previous studies of ISEE-1, GEOS-2, and Polar PWI data, which used the WDF method to show that oblique plasmaspheric hiss was observed only at larger L shells within the plasmasphere (e.g., Hayakawa et al., 1986; Hayakawa & Sazhin, 1992; Storey et al., 1991) but in some cases was predominantly field aligned at L shells between 3.6 and 4.2 (e.g., Santolík et al., 2001). Investigation of the secondary oblique population of plasmaspheric hiss reveals that waves in this mode occur more readily during low geomagnetic activity, with occurrence rates generally decreasing with increasing activity.

The results of this study indicate that inside $L = 3.0$ the primary wave population spans the entire plasmaspheric hiss frequency range (100 Hz to 5 kHz), while the secondary population only exists at frequencies with $f/f_{ce}$ greater than 0.01, or $f > 700$ Hz. At these frequencies, the secondary population possesses weaker magnetic field power spectral density and stronger electric field power spectral density in comparison to the primary wave population. This is consistent with what one would expect for larger wave normal angles close to the resonance cone.

The oblique secondary wave population is generally confined between 19:00 and 9:00 MLT, a structure that is similar to that observed for obliquely propagating chorus waves in the equatorial region (Li et al., 2016), although at markedly different L shells. This suggests a causal link between obliquely propagating equatorial chorus and obliquely propagating plasmaspheric hiss waves at low L shells (in keeping with existing theory of chorus as the source of both field-aligned and oblique plasmaspheric hiss). The plausibility of this link has been tested using the HOTRAY ray tracing code, with results indicating that it is indeed viable for chorus waves

generated at oblique angles to become field aligned at high latitudes before entering the plasmasphere to be observed as oblique plasmaspheric hiss at low L shells. This explanation is also compatible with the observed variation of the oblique secondary plasmaspheric hiss population with geomagnetic activity. An increase in Landau resonant electrons, typically associated with elevated substorm activity, cause chorus waves to be more substantially damped outside of the plasmasphere, hence stunting the amount of chorus wave power that can access the plasmasphere and evolve into oblique plasmaspheric hiss. As such, the theory of chorus as the source of plasmaspheric hiss remains plausible despite the discrepancies between previous observational results (bimodal wave normal angle distribution only apparent in the outer plasmasphere) and the statistical results from the Van Allen Probes presented in this study (bimodal wave normal angle distribution only apparent deep inside of the plasmasphere).

These new results highlight the variable distribution in both power spectral density and wave normal angle of two discrete plasmaspheric hiss wave modes. These factors must be considered in future studies if we are to gain a more complete understanding of the impact of particle interactions with plasmaspheric hiss, particularity obliquely propagating plasmaspheric hiss with a strong electric field signature (e.g., Albert, 2017; Mourenas et al., 2014).

**Acknowledgments**
This work was performed under the support of JHU/APL contract 921647 under NASA Prime contract NAS5-01072. EMFISIS data may be obtained from http://emfisis.physics.uiowa.edu/data/index. O. S. acknowledges support from grants LTAUSA17070, GACR17-07027S, and from the Praemium Academiae award. L. C. acknowledge NSF grant 1405041 through the Geospace Environment Modeling program. R. B. H. acknowledges support from the Natural Environment Research Council grant NE/P01738X/1 (Rad-Sat).

## References

Albert, J. M. (2017). Quasi-linear diffusion coefficients for highly oblique whistler mode waves. *Journal of Geophysical Research: Space Physics*, *122*, 5339–5354. https://doi.org/10.1002/2017JA024124

Abel, B., & Thorne, R. M. (1998). Electron scattering loss in Earth's inner magnetosphere: 1. Dominant physical processes. *Journal of Geophysical Research*, *103*(A2), 2385–2396. https://doi.org/10.1029/97JA02919

Bortnik, J., Chen, L., Li, W., Thorne, R. M., & Horne, R. B. (2011). Modeling the evolution of chorus waves into plasmaspheric hiss. *Journal of Geophysical Research*, *116*, A08221. https://doi.org/10.1029/2011JA016499

Bortnik, J., Chen, L., Li, W., Thorne, R. M., Meredith, N. P., & Horne, R. B. (2011). Modeling the wave power distribution and characteristics of plasmaspheric hiss. *Journal of Geophysical Research*, *116*, A12209. https://doi.org/10.1029/2011JA016862

Bortnik, J., Chen, L., Li, W., Thorne, R. M., Nishimura, Y., Angelopoulos, V., & Kletzing, C. A. (2016). Relationship between chorus and plasmaspheric hiss waves. In A. Keiling, D.-H. Lee, & V. Nakariakov (Eds.), *Low-frequency Waves in Space Plasmas*. Hoboken, NJ: John Wiley Inc. https://doi.org/10.1002/9781119055006.ch6

Bortnik, J., Li, W., Thorne, R. M., Angelopoulos, V., Cully, C., Bonnell, J., et al. (2009). An observation linking the origin of plasmaspheric hiss to discrete chorus emissions. *Science*, *324*(5928), 775–778. https://doi.org/10.1126/science.1171273

Bortnik, J., Thorne, R. M., & Meredith, N. P. (2008). The unexpected origin of plasmaspheric hiss from discrete chorus emissions. *Nature*, *452*(7183), 62–66. https://doi.org/10.1038/nature06741

Chan, K.-W., & Holzer, R. E. (1976). ELF hiss associated with plasma density enhancements in the outer magnetosphere. *Journal of Geophysical Research*, *81*(13), 2267–2274. https://doi.org/10.1029/JA081i013p02267

Chen, L., Bortnik, J., Li, W., Thorne, R. M., & Horne, R. B. (2012a). Modeling the properties of plasmaspheric hiss: 1. Dependence on chorus wave emission. *Journal of Geophysical Research*, *117*, A05201. https://doi.org/10.1029/2011JA017201

Chen, L., Bortnik, J., Li, W., Thorne, R. M., & Horne, R. B. (2012b). Modeling the properties of plasmaspheric hiss: 2. Dependence on the plasma density distribution. *Journal of Geophysical Research*, *117*, A05202. https://doi.org/10.1029/2011JA017202

Chen, L., Li, W., Bortnik, J., & Thorne, R. M. (2012). Amplification of whistler-mode hiss inside the plasmasphere. *Geophysical Research Letters*, *39*, L08111. https://doi.org/10.1029/2012GL051488

Chum, J., & Santolik, O. (2005). Propagation of whistler-mode chorus to low altitudes: Divergent ray trajectories and ground accessibility. *Annales Geophysicae*, *23*, 3727–3738. https://doi.org/10.5194/angeo-23-3727-2005

Church, S. R., & Thorne, R. M. (1983). On the origin of plasmaspheric hiss: Ray path integrated amplification. *Journal of Geophysical Research*, *88*(A10), 7941–7957. https://doi.org/10.1029/JA088iA10p07941

Draganov, A. B., Inan, U. S., Sonwalkar, V. S., & Bell, T. F. (1992). Magnetospherically reflected whistlers as a source of plasmaspheric hiss. *Geophysical Research Letters*, *19*, 233–236. https://doi.org/10.1029/91GL03167

Dunckel, N., & Helliwell, R. A. (1969). Whistler-mode emissions on the OGO 1 satellite. *Journal of Geophysical Research*, *74*(26), 6371–6385. https://doi.org/10.1029/JA074i026p06371

Gendrin, R. (1961). Le guidage des whistlers par le champ magnetique. *Planetary and Space Science*, *5*, 274–278. https://doi.org/10.1016/0032-0633(61)90096-4

Hartley, D. P., Chen, Y., Kletzing, C. A., Denton, M. H., & Kurth, W. S. (2015). Applying the cold plasma dispersion relation to whistler mode chorus waves: EMFISIS wave measurements from the Van Allen Probes. *Journal of Geophysical Research: Space Physics*, *120*, 1144–1152. https://doi.org/10.1002/2014JA020808

Hartley, D. P., Kletzing, C. A., Kurth, W. S., Bounds, S. R., Averkamp, T. F., Hospodarsky, G. B., et al. (2016). Using the cold plasma dispersion relation and whistler mode waves to quantify the antenna sheath impedance of the Van Allen Probes EFW instrument. *Journal of Geophysical Research: Space Physics*, *121*, 4590–4606. https://doi.org/10.1002/2016JA022501

Hartley, D. P., Kletzing, C. A., Kurth, W. S., Hospodarsky, G. B., Bounds, S. R., Averkamp, T. F., et al. (2017). An improved sheath impedance model for the Van Allen Probes EFW instrument: Effects of the spin axis antenna. *Journal of Geophysical Research: Space Physics*, *122*, 4420–4429. https://doi.org/10.1002/2016JA023597

Hayakawa, M., Ohmi, N., Parrot, M., & Lefeuvre, F. (1986). Direction finding of ELF hiss emissions in a detached plasma region of the magnetosphere. *Journal of Geophysical Research*, *91*(A1), 135–141. https://doi.org/10.1029/JA091iA01p00135

Hayakawa, M., & Sazhin, S. S. (1992). Mid-latitude and plasmaspheric hiss: A review. *Planetary and Space Science*, *40*(10), 1325–1338. https://doi.org/10.1016/0032-0633(92)90089-7

Horne, R. B. (1989). Path-integrated growth of electrostatic waves: The generation of terrestrial myriametric radiation. *Journal of Geophysical Research*, *94*(A7), 8895–8909. https://doi.org/10.1029/JA094iA07p08895

Huang, C. Y., Goertz, C. K., & Anderson, R. R. (1983). A theoretial study of plasmaspheric hiss generation. *Journal of Geophysical Research*, *88*, 7927–7940. https://doi.org/10.1029/JA088iA10p07927

Kletzing, C. A., Kurth, W. S., Acuna, M., MacDowall, R. J., Torbert, R. B., Averkamp, T., et al. (2013). The Electric and Magnetic Field Instrument Suite and Integrated Science (EMFISIS) on RBSP. *Space Science Reviews*, *179*, 127–181. https://doi.org/10.1007/s11214-013-9993-6

Kurth, W. S., De Pascuale, S., Faden, J. B., Kletzing, C. A., Hospodarsky, G. B., Thaller, S., et al. (2015). Electron densities inferred from plasma wave spectra obtained by the Waves instrument on Van Allen Probes. *Journal of Geophysical Research: Space Physics*, *120*, 904–914. https://doi.org/10.1002/2014JA020857

Li, W., Chen, L., Bortnik, J., Thorne, R. M., Angelopoulos, V., Kletzing, C. A., et al. (2015). First evidence for chorus at a large geocentric distance as a source of plasmaspheric hiss: Coordinated THEMIS and Van Allen Probes observation. *Geophysical Research Letters*, *42*, 241–248. https://doi.org/10.1002/2014GL062832

Li, W., Santolik, O., Bortnik, J., Thorne, R. M., Kletzing, C. A., Kurth, W. S., et al. (2016). New chorus wave properties near the equator from Van Allen Probes wave observations. *Geophysical Research Letters*, *43*, 4725–4735. https://doi.org/10.1002/2016GL068780

Li, W., Thorne, R. M., Bortnik, J., Nishimura, Y., Angelopoulos, V., Chen, L., et al. (2010). Global distributions of suprathermal electrons observed on THEMIS and potential mechanisms for access into the plasmasphere. *Journal of Geophysical Research*, *115*, A00J10. https://doi.org/10.1029/2010JA015687

Lyons, L. R., & Thorne, R. M. (1973). Equilibrium structure of radiation belt electrons. *Journal of Geophysical Research*, *78*(13), 2142–2149. https://doi.org/10.1029/JA078i013p02142

Lyons, L. R., Thorne, R. M., & Kennel, C. F. (1972). Pitch-angle diffusion of radiation belt electrons within the plasmasphere. *Journal of Geophysical Research*, *77*(19), 3455–3474. https://doi.org/10.1029/JA077i019p03455

Meredith, N. P., Horne, R. B., Bortnik, J., Thorne, R. M., Chen, L., Li, W., et al. (2013). Global statistical evidence for chorus as the embryonic source of plasmaspheric hiss. *Geophysical Research Letters*, *40*, 2891–2896. https://doi.org/10.1002/grl.50593

Meredith, N. P., Horne, R. B., Clilverd, M. A., Horsfall, D., Thorne, R. M., & Anderson, R. R. (2006). Origins of plasmaspheric hiss. *Journal of Geophysical Research*, *111*, A09217. https://doi.org/10.1029/2006JA011707

Meredith, N. P., Horne, R. B., Thorne, R. M., Summers, D., & Anderson, R. R. (2004). Substorm dependence of plasmaspheric hiss. *Journal of Geophysical Research*, *109*, A06209. https://doi.org/10.1029/2004JA010387

Mourenas, D., Artemyev, A. V., Agapitov, O. V., & Krasnoselskikh, V. (2014). Consequences of geomagnetic activity on energization and loss of radiation belt electrons by oblique chorus waves. *Journal of Geophysical Research: Space Physics*, *119*, 2775–2796. https://doi.org/10.1002/2013JA019674

Nakamura, S., Omura, Y., Summers, D., & Kletzing, C. A. (2016). Observational evidence of the nonlinear wave growth theory of plasmaspheric hiss. *Geophysical Research Letters*, *43*, 10,040–10,049. https://doi.org/10.1002/2016GL070333

Omura, Y., Nakamura, S., Kletzing, C. A., Summers, D., & Hikishima, M. (2015). Nonlinear wave growth theory of coherent hiss emissions in the plasmasphere. *Journal of Geophysical Research: Space Physics*, *120*, 7642–7657. https://doi.org/10.1002/2015JA021520

Russell, C. T., Holzer, R. E., & Smith, E. J. (1969). OGO 3 observations of ELF noise in the magnetosphere: 1. Spatial extent and frequency of occurrence. *Journal of Geophysical Research*, *74*(3), 755–777. https://doi.org/10.1029/JA074i003p00755

Santolík, O., Chum, J., Parrot, M., Gurnett, D. A., Pickett, J. S., & Cornilleau-Wehrlin, N. (2006). Propagation of whistler mode chorus to low altitudes: Spacecraft observations of structured ELF hiss. *Journal of Geophysical Research*, *111*, A10208. https://doi.org/10.1029/2005JA011462

Santolík, O., Macúšová, E., Kolmašová, I., Cornilleau-Wehrlin, N., & de Conchy, Y. (2014). Propagation of lower-band whistler-mode waves in the outer Van Allen belt: Systematic analysis of 11 years of multi-component data from the Cluster spacecraft. *Geophysical Research Letters*, *41*, 2729–2737. https://doi.org/10.1002/2014GL059815

Santolík, O., Parrot, M., & Lefeuvre, F. (2003). Singular value decomposition methods for wave propagation analysis. *Radio Science*, *38*(1), 1010. https://doi.org/10.1029/2000RS002523

Santolík, O., Parrot, M., Storey, L. R. O., Pickett, J. S., & Gurnett, D. A. (2001). Propagation analysis of plasmaspheric hiss using Polar PWI measurements. *Geophysical Research Letters*, *28*, 1127–1130. https://doi.org/10.1029/2000GL012239

Santolík, O., Pickett, J. S., Gurnett, D. A., & Storey, L. R. O. (2002). Magnetic component of narrowband ion cyclotron waves in the auroral zone. *Journal of Geophysical Research*, *107*(A12), 1444. https://doi.org/10.1029/2001JA000146

Selesnick, R. S., Blake, J. B., & Mewaldt, R. A. (2003). Atmospheric losses of radiation belt electrons. *Journal of Geophysical Research*, *108*(A12), 1468. https://doi.org/10.1029/2003JA010160

Smith, E. J., Frandsen, A. M. A., Tsurutani, B. T., Thorne, R. M., & Chan, K. W. (1974). Plasmaspheric hiss intensity variations during magnetic storms. *Journal of Geophysical Research*, *79*(16), 2507–2510. https://doi.org/10.1029/JA079i016p02507

Solomon, J., Cornilleau-Wehrlin, N., Korth, A., & Kremser, G. (1988). An experimental study of ELF/VLF hiss generation in the Earth's magnetosphere. *Journal of Geophysical Research*, *93*, 1839–1847. https://doi.org/10.1029/JA093iA03p01839

Storey, L. R. O., Lefeuvre, F., Parrot, M., Cairó, L., & Anderson, R. R. (1991). Initial survey of the wave distribution functions for plasmaspheric hiss observed by ISEE 1. *Journal of Geophysical Research*, *96*(A11), 19,469–19,489. https://doi.org/10.1029/91JA01828

Summers, D., Ni, B., Meredith, N. P., Horne, R. B., Thorne, R. M., Moldwin, M. B., et al. (2008). Electron scattering by whistler-mode ELF hiss in plasmaspheric plumes. *Journal of Geophysical Research*, *113*, A04219. https://doi.org/10.1029/2007JA012678

Summers, D., Omura, Y., Nakamura, S., & Kletzing, C. A. (2014). Fine structure of plasmaspheric hiss. *Journal of Geophysical Research: Space Physics*, *119*, 9134–9149. https://doi.org/10.1002/2014JA020437

Thorne, R. M., Church, S. R., Malloy, W. J., & Tsurutani, B. T. (1977). The local time variation of ELF emissions during periods of substorm activity. *Journal of Geophysical Research*, *82*(10), 1585–1590. https://doi.org/10.1029/JA082i010p01585

Thorne, R. M., Smith, E. J., Burton, R. K., & Holzer, R. E. (1973). Plasmaspheric hiss. *Journal of Geophysical Research*, *78*(10), 1581–1596. https://doi.org/10.1029/JA078i010p01581

Thorne, R. M., Smith, E. J., Fiske, K. J., & Church, S. R. (1974). Intensity variation of ELF hiss and chorus during isolated substorms. *Geophysical Research Letters*, *1*, 193–196. https://doi.org/10.1029/GL001i005p00193

Yu, J., Li, L. Y., Cao, J. B., Chen, L., Wang, J., & Yang, J. (2017). Propagation characteristics of plasmaspheric hiss: Van Allen Probe observations and global empirical models. *Journal of Geophysical Research: Space Physics*, *122*, 4156–4167. https://doi.org/10.1002/2016JA023372